Prandtl number scaling of unsteady natural convection boundary layers for Pr > 1 fluids under isothermal heating

Wenxian Lin,[1,2,*] S. W. Armfield,[3] J. C. Patterson,[1] and Chengwang Lei[1]
[1]*School of Engineering, James Cook University, Townsville, Queensland 4811, Australia*
[2]*Solar Energy Research Institute, Yunnan Normal University, Kunming, Yunnan 650092, People's Republic of China*
[3]*School of Aerospace, Mechanical and Mechatronic Engineering, University of Sydney, New South Wales 2006, Australia*
(Received 7 October 2008; published 24 June 2009)

In this paper, the scalings incorporating the Prandtl number (Pr) dependence have been obtained by a scaling analysis for the unsteady natural convection boundary layer of an initially quiescent isothermal Newtonian fluid of Pr > 1 produced by the sudden imposition of a higher temperature on a vertical plate. It is shown that the transient flow behavior of the resulting boundary layer can be described by a three-region structure and at the start-up stage the boundary layer development is one dimensional and independent of height due to the dominance of pure conduction; however, at steady state it becomes two dimensional and height dependent as the flow becomes dominated by convection. Numerical results demonstrate that the scalings representing the thermal boundary layer development accurately represent their Pr dependence over the whole stage of flow development. The scalings representing the viscous boundary layer development are generally in good agreement with the numerical results with the Pr variation over the whole stage of flow development, although there are small deviations from the numerical results with the Pr variation that are within acceptable limits for scaling.

DOI: 10.1103/PhysRevE.79.066313 PACS number(s): 44.25.+f, 47.55.P−, 44.20.+b, 47.15.Cb

I. INTRODUCTION

Natural convection boundary layer flow has been a classic problem in fluid mechanics and heat transfer due to its fundamental and practical significance. It has attracted extensive experimental, analytical, and numerical studies. The majority of the earlier studies have focused on the experimental and analytical explorations of the steady-state behavior of the flow, particularly that in a rectangular cavity with differentially heated sidewalls, as reviewed by Catton [1], Ostrach [2], Gebhart *et al.* [3], and Hyun [4], and more recently as summarized regularly in the literature reviews on heat transfer (see, e.g., Goldstein *et al.* [5]).

The transient flow behavior of unsteady natural convection boundary layers is also of fundamental interest and practical importance. Patterson and Imberger [6] conducted the pioneering scaling analysis on the transient behavior of flow when the opposing two vertical sidewalls of a two-dimensional rectangular cavity are impulsively heated and cooled by an equal amount. They devised a classification of the flow development through several transient flow regimes to one of three steady-state types of flow based on the relative values of the Rayleigh number Ra, the Prandtl number Pr, and the aspect ratio of cavity A. Since then, extensive investigations have been made for many aspects of unsteady natural convection boundary layer flow under various flow configurations through scaling analysis, numerical simulation, and experiments, as recently reviewed by Lin *et al.* [7].

Although the scalings obtained from scaling analysis have been shown to correctly predict their Ra and A dependence under various flow configurations (see, e.g., [6–11]), it has also been shown that some of the scalings do not perform satisfactorily with Pr variation. This prompts us to develop improved scalings by taking into account the Pr variation in the scaling analysis. In this study, improved scalings with Pr variation will be developed from the scaling analysis for the unsteady natural convection boundary layers of Pr > 1 fluids under isothermal heating conditions. Companion studies have also been made for the unsteady natural convection boundary layers of Pr > 1 fluids under ramp heating conditions [12] and for the steady-state natural convection boundary layers of Pr > 1 fluids under isoflux heating conditions [13].

The remainder of this paper is organized as follows. The scaling analysis is carried out in Sec. II to develop improved scalings with Pr variation. These scalings and the governing equations are made dimensionless in Sec. III and then validated and analyzed with a series of direct numerical simulation results with Pr variation in Sec. IV. Finally, conclusions are made in Sec. V.

II. SCALING ANALYSIS

Under consideration is the transient flow behavior resulting from heating a quiescent isothermal Newtonian fluid with Pr > 1 by imposing a fixed higher temperature, T_w, on a vertical plate of length H. The fluid is initially at rest and at a uniform temperature $T_0 (T_0 < T_w)$. It is assumed that the flow is laminar.

The governing equations of motion are the Navier-Stokes equations with the Boussinesq approximation for buoyancy, which together with the temperature equation can be written in the following two-dimensional forms:

$$\frac{\partial U}{\partial X} + \frac{\partial V}{\partial Y} = 0, \tag{1}$$

*FAX: 61-7-4781-6788; wenxian.lin@jcu.edu.au

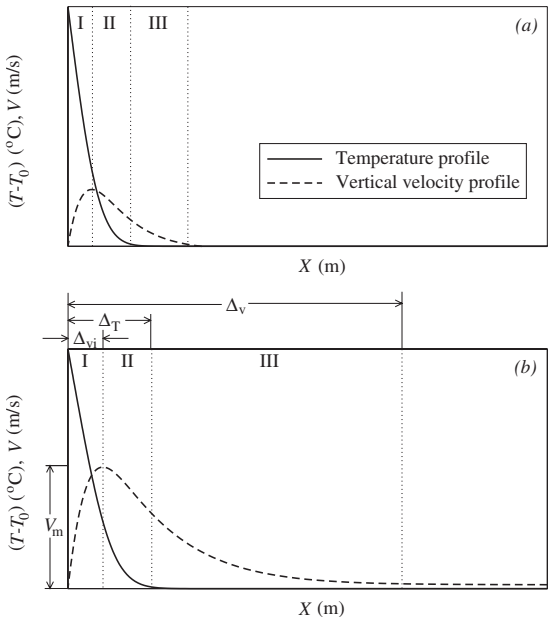

FIG. 1. Numerically simulated horizontal profiles of temperature and vertical velocity at dimensionless height $y=Y/H=0.5$ within a natural convection boundary layer: (a) at the start-up stage (at dimensionless time $\tau=0.5$) and (b) at steady state (at dimensionless time $\tau=10$) for Pr=10 and Ra=10^8, where τ and y are defined by Eq. (33).

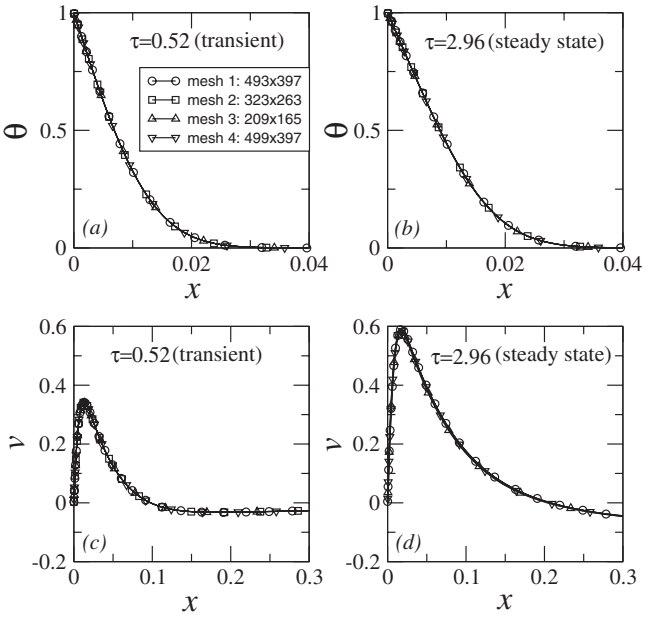

FIG. 2. Numerically simulated horizontal profiles of dimensionless temperature θ and dimensionless vertical velocity v at dimensionless height $y=0.5$ for Ra=10^8 and Pr=50 with four different meshes. Meshes 1–3 are for the 2×1 computational domain and mesh 4 is for the 4×1 computational domain.

$$\frac{\partial U}{\partial t}+\frac{\partial(UU)}{\partial X}+\frac{\partial(VU)}{\partial Y}=-\frac{1}{\rho}\frac{\partial P}{\partial X}+\nu\left(\frac{\partial^2 U}{\partial X^2}+\frac{\partial^2 U}{\partial Y^2}\right), \quad (2)$$

$$\frac{\partial V}{\partial t}+\frac{\partial(UV)}{\partial X}+\frac{\partial(VV)}{\partial Y}=-\frac{1}{\rho}\frac{\partial P}{\partial Y}+\nu\left(\frac{\partial^2 V}{\partial X^2}+\frac{\partial^2 V}{\partial Y^2}\right)+g\beta(T-T_0), \quad (3)$$

$$\frac{\partial T}{\partial t}+\frac{\partial(UT)}{\partial X}+\frac{\partial(VT)}{\partial Y}=\kappa\left(\frac{\partial^2 T}{\partial X^2}+\frac{\partial^2 T}{\partial Y^2}\right), \quad (4)$$

where U and V are the horizontal (X direction) and vertical (Y direction) velocity components, t is time, P is pressure, T is temperature, g is the acceleration due to gravity, and β, ν, and κ are the thermal expansion coefficient, kinematic viscosity, and thermal diffusivity of the fluid at the temperature T_0, respectively. Gravity acts in the negative Y direction.

For the unsteady natural convection boundary layer flow considered here, the major governing parameters are the Rayleigh number Ra and the Prandtl number Pr defined as

$$\mathrm{Ra}=\frac{g\beta\Delta T H^3}{\nu\kappa}, \quad \mathrm{Pr}=\frac{\nu}{\kappa}, \quad (5)$$

where $\Delta T=T_W-T_0$.

The basic procedure described in [6] is followed here modified appropriately to include the dependence on Pr correctly by examining in more detail the various balances in the governing equations. With the initiation of the flow, a vertical boundary layer will be developed adjacent to the vertical plate which will experience a start-up stage dominated by one-dimensional conduction followed by a short transitional stage at which traveling waves due to the leading edge effect are present and the one-dimensional conduction transits to two-dimensional convection before reaching steady state [7,14,15].

The forcing for the vertical boundary layer is from conduction of heat through the wall. The ratio of the unsteady term $(\Delta T/t)$ to the convection term $(V\Delta T/H)$ in the temperature Eq. (4) is $O(H/Vt)$, and for sufficiently small t this is much larger than 1, so the initial balance is between the heat conducted in through the wall (i.e., the term $\kappa\Delta T/\Delta_T^2$) and the unsteady term, which leads to the following scaling for the thermal boundary layer thickness Δ_T at the start-up stage:

$$\Delta_T \sim \kappa^{1/2}t^{1/2}. \quad (6)$$

Hence, a gradient in temperature exists from the vertical sidewall to a distance Δ_T.

The buoyancy forces resulting from this heating act to accelerate the flow over the thickness Δ_T only. In this region, the ratio of the inertial term to the viscous term in the vertical momentum Eq. (3) is $O[(V/t)/(\nu V/\Delta_T^2)]\sim O(\Delta_T^2/\nu t)\sim O(1/\mathrm{Pr})$ as $\Delta_T\sim\kappa^{1/2}t^{1/2}$ as shown in Eq. (6), which is much smaller than 1 for $\mathrm{Pr}\gg1$, so that the balance over Δ_T is between the viscous term $(\nu\partial^2V/\partial X^2)$ and the buoyancy term $(g\beta\Delta T)$.

The peak velocity V_m must occur within Δ_T. Suppose V_m is at a distance Δ_{vi} from the wall. Also for $\mathrm{Pr}>1$ there will be a region of flow outside Δ_T where there is flow that is not directly forced by buoyancy but is the result of diffusion of momentum as the result of viscosity. Suppose this is Δ_v from the wall. Hence a three-region structure as shown in Fig. 1

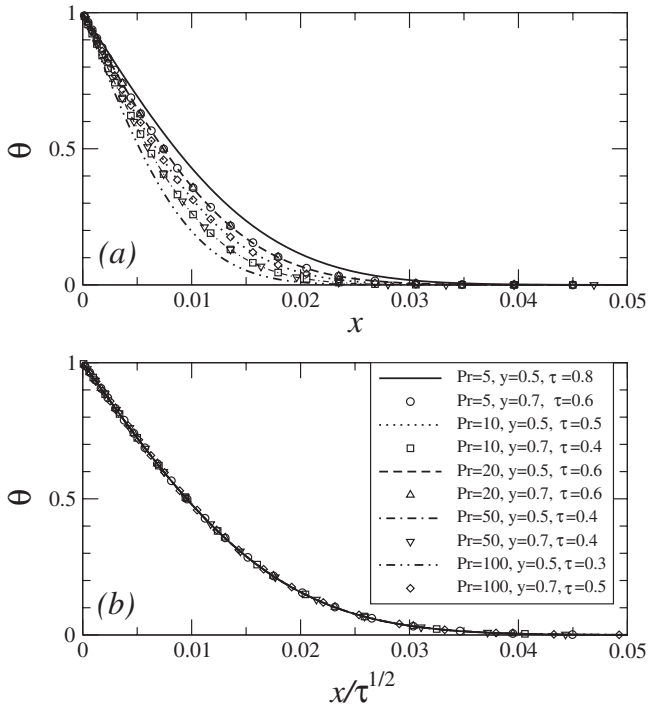

FIG. 3. Horizontal profiles of dimensionless temperature θ at dimensionless heights $y=0.5$ and $y=0.7$ for different Pr at the start-up stage: (a) raw data and (b) θ plotted against $x/\tau^{1/2}$ (dimensionless).

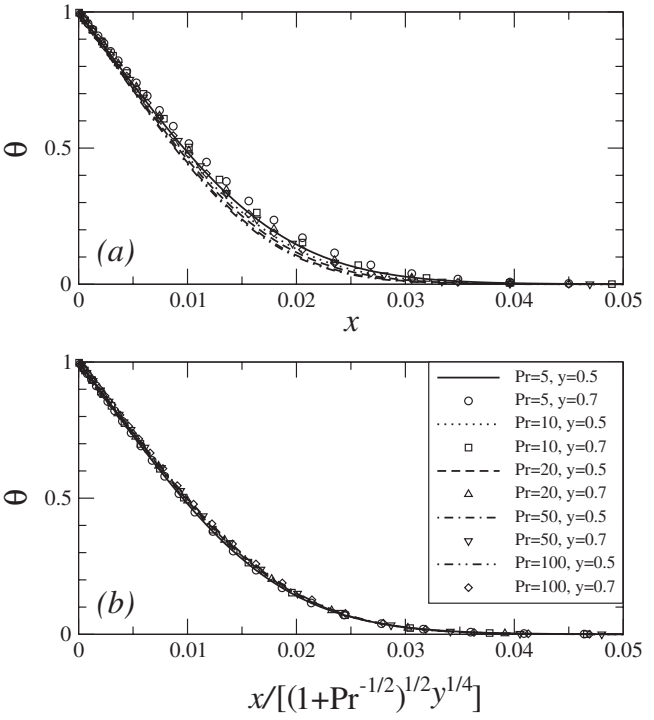

FIG. 4. Horizontal profiles of dimensionless temperature θ at dimensionless heights $y=0.5$ and $y=0.7$ for different Pr at steady state: (a) raw data and (b) θ plotted against $x/[(1+\mathrm{Pr}^{-1/2})^{1/2}y^{1/4}]$ (dimensionless).

can be depicted for the natural convection boundary layers of $\mathrm{Pr}>1$ fluids.

In regions I and II, the balance is between viscosity and buoyancy, i.e.,

$$0 \sim \nu\frac{\partial^2 V}{\partial X^2} + g\beta\Delta T. \tag{7}$$

However, in region III the balance is between viscosity and inertia, since there is no buoyancy there.

In region I, balance (7) gives

$$\nu\frac{V_m}{\Delta_{vi}^2} \sim g\beta\Delta T, \tag{8}$$

i.e.,

$$V_m \sim \frac{g\beta\Delta T}{\nu}\Delta_{vi}^2. \tag{9}$$

In region II, the forcing is over the distance $(\Delta_T-\Delta_{vi})$ but the gradient of V is over $(\Delta_v-\Delta_{vi})$. The best way to look at this is to integrate the vertical momentum equation over region II, giving

$$0 \sim \nu\left(\frac{\partial V}{\partial X}\right)_{\Delta_{vi}}^{\Delta_T} + g\beta\int_{\Delta_{vi}}^{\Delta_T} T dX. \tag{10}$$

Since $(\partial V/\partial X)_{\Delta_{vi}}=0$ (that is where the maximum is) and approximating $(\partial V/\partial X)_{\Delta T}\sim V_m/(\Delta_v-\Delta_{vi})$ and $\int_{\Delta_{vi}}^{\Delta_T} T dx \sim \Delta T(\Delta_T-\Delta_{vi})$, this gives

$$\nu\frac{V_m}{\Delta_v-\Delta_{vi}} \sim g\beta\Delta T(\Delta_T-\Delta_{vi}). \tag{11}$$

Hence,

$$V_m \sim \frac{g\beta\Delta T}{\nu}(\Delta_T-\Delta_{vi})(\Delta_v-\Delta_{vi}). \tag{12}$$

Matching this with Eq. (9) obtained above for V_m gives

$$(\Delta_T-\Delta_{vi})(\Delta_v-\Delta_{vi}) \sim \Delta_{vi}^2, \tag{13}$$

so that

$$\Delta_T\Delta_v - (\Delta_T+\Delta_v)\Delta_{vi} + \Delta_{vi}^2 \sim \Delta_{vi}^2, \tag{14}$$

which leads to

$$\Delta_{vi} \sim \frac{\Delta_T\Delta_v}{\Delta_T+\Delta_v}. \tag{15}$$

In region III, as there is no buoyancy force, the flow is driven solely by diffusion of momentum, meaning that the unsteady term balances the viscous term, giving

$$\frac{V}{t} \sim \nu\frac{V}{\Delta_v^2}. \tag{16}$$

This leads to

$$\Delta_v \sim \nu^{1/2}t^{1/2} \sim \mathrm{Pr}^{1/2}\,\Delta_T, \tag{17}$$

which is the scaling for Δ_v at the start-up stage. Hence, scaling (15) becomes

$$\Delta_{vi} \sim \frac{\mathrm{Pr}^{1/2}}{1+\mathrm{Pr}^{1/2}}\Delta_T \sim \frac{1}{1+\mathrm{Pr}^{-1/2}}\Delta_T \sim \frac{1}{1+\mathrm{Pr}^{-1/2}}\kappa^{1/2}t^{1/2}. \tag{18}$$

This is the scaling for Δ_{vi} at the start-up stage.

So scaling (9) for V_m becomes

$$V_m \sim \frac{g\beta\Delta T}{\nu}\Delta_{vi}^2 \sim \frac{g\beta\Delta T}{\nu}\left(\frac{1}{1+\mathrm{Pr}^{-1/2}}\right)^2\Delta_T^2. \tag{19}$$

Since $\Delta_T \sim \kappa^{1/2}t^{1/2}$, this leads to

$$V_m \sim \frac{g\beta\Delta T}{\nu}\left(\frac{1}{1+\mathrm{Pr}^{-1/2}}\right)^2\kappa t \sim \frac{\mathrm{Ra}\kappa^2}{H^3}\left(\frac{1}{1+\mathrm{Pr}^{-1/2}}\right)^2 t, \tag{20}$$

which is the scaling for V_m at the start-up stage.

The boundary layer will continue to grow until convection of heat carried away by the flow balances the conduction of heat transferred in through the wall and the development of the boundary layer reaches steady state. At a height Y, this happens at

$$\frac{V_m\Delta T}{Y} \sim \kappa\frac{\Delta T}{\Delta_T^2}, \tag{21}$$

i.e.,

$$\frac{\mathrm{Ra}\kappa^2}{H^3 Y}\left(\frac{1}{1+\mathrm{Pr}^{-1/2}}\right)^2 t \sim \kappa\frac{1}{\kappa t}. \tag{22}$$

This leads to

$$t^2 \sim \frac{H^3 Y}{\mathrm{Ra}\kappa^2}(1+\mathrm{Pr}^{-1/2})^2, \tag{23}$$

which gives the following scaling for the time when the boundary layer reaches steady state:

$$t_s \sim \frac{H^2}{\mathrm{Ra}^{1/2}\kappa}\left(\frac{Y}{H}\right)^{1/2}(1+\mathrm{Pr}^{-1/2}). \tag{24}$$

The corresponding scaling for the steady-state maximum velocity from Eq. (20) is

$$V_{ms} \sim \frac{\mathrm{Ra}\kappa^2}{H^3}\left(\frac{1}{1+\mathrm{Pr}^{-1/2}}\right)^2 t_s \sim \frac{\mathrm{Ra}^{1/2}\kappa}{H}\left(\frac{Y}{H}\right)^{1/2}\frac{1}{(1+\mathrm{Pr}^{-1/2})}. \tag{25}$$

The scaling for the steady-state thermal boundary layer thickness from Eq. (6) is

$$\Delta_{Ts} \sim \kappa^{1/2}t_s^{1/2} \sim \frac{H}{\mathrm{Ra}^{1/4}}\left(\frac{Y}{H}\right)^{1/4}(1+\mathrm{Pr}^{-1/2})^{1/2}. \tag{26}$$

The scaling for the steady-state inner viscous boundary layer thickness from Eq. (18) is

$$\Delta_{vis} \sim \frac{1}{1+\mathrm{Pr}^{-1/2}}\Delta_{Ts} \sim \frac{H}{\mathrm{Ra}^{1/4}}\left(\frac{Y}{H}\right)^{1/4}\frac{1}{(1+\mathrm{Pr}^{-1/2})^{1/2}}. \tag{27}$$

The scaling for the steady-state whole viscous boundary layer thickness from Eq. (17) is

$$\Delta_{vs} \sim \mathrm{Pr}^{1/2}\,\Delta_{Ts} \sim \frac{H}{\mathrm{Ra}^{1/4}}\left(\frac{Y}{H}\right)^{1/4}\mathrm{Pr}^{1/2}(1+\mathrm{Pr}^{-1/2})^{1/2}. \tag{28}$$

III. NONDIMENSIONAL FORMULATION

To facilitate the numerical validation of the scalings obtained above, the dimensionless forms of the governing equations and the scalings are used. For the natural convection boundary layer flows considered here, it is natural to choose H, the height of the plate, as the characteristic length scale. From Eq. (25), it is also natural to choose $V_0 = \kappa\mathrm{Ra}^{1/2}/H$ as the characteristic velocity scale. Hence, the characteristic time scale for the flows is apparently (H/V_0) and the characteristic pressure scale is ρV_0^2. It is also apparent that $\Delta T = T_w - T_0$ is the characteristic temperature difference scale.

With these characteristic scales, governing equations (1)–(4) can be written in the following nondimensional forms:

$$\frac{\partial u}{\partial x} + \frac{\partial v}{\partial y} = 0, \tag{29}$$

$$\frac{\partial u}{\partial \tau} + \frac{\partial (uu)}{\partial x} + \frac{\partial (vu)}{\partial y} = -\frac{\partial p}{\partial x} + \frac{\mathrm{Pr}}{\mathrm{Ra}^{1/2}}\left(\frac{\partial^2 u}{\partial x^2} + \frac{\partial^2 u}{\partial y^2}\right), \tag{30}$$

$$\frac{\partial v}{\partial \tau} + \frac{\partial (uv)}{\partial x} + \frac{\partial (vv)}{\partial y} = -\frac{\partial p}{\partial y} + \frac{\mathrm{Pr}}{\mathrm{Ra}^{1/2}}\left(\frac{\partial^2 v}{\partial x^2} + \frac{\partial^2 v}{\partial y^2}\right) + \mathrm{Pr}\;\theta, \tag{31}$$

$$\frac{\partial \theta}{\partial \tau} + \frac{\partial (u\theta)}{\partial x} + \frac{\partial (v\theta)}{\partial y} = \frac{1}{\mathrm{Ra}^{1/2}}\left(\frac{\partial^2 \theta}{\partial x^2} + \frac{\partial^2 \theta}{\partial y^2}\right), \tag{32}$$

where x, y, u, v, τ, p, and θ are, respectively, the dimensionless forms of X, Y, U, V, t, P, and T,which are made dimensionless by their respective characteristic scales, i.e.,

$$x = \frac{X}{H}, \quad y = \frac{Y}{H}, \quad u = \frac{U}{V_0}, \quad v = \frac{V}{V_0}, \quad \tau = \frac{t}{(H/V_0)},$$
$$p = \frac{P}{\rho V_0^2}, \quad \theta = \frac{T - T_0}{T_w - T_0}. \tag{33}$$

The origin of the coordinate system is located at the leading edge of the heated plate, at $x=0$, $y=0$.

The scalings obtained above are made dimensionless as follows. At the start-up stage, scalings (6), (17), (18), and (20) can be written in dimensionless form as

$$\delta_T = \frac{\Delta_T}{H} \sim \frac{\kappa^{1/2}t^{1/2}}{H} \sim \frac{\kappa^{1/2}[(H/V_0)\tau]^{1/2}}{H} \sim \left(\frac{\kappa}{V_0 H}\right)^{1/2}\tau^{1/2} \sim \frac{\tau^{1/2}}{\mathrm{Ra}^{1/4}}, \tag{34}$$

$$\delta_v = \frac{\Delta_v}{H} \sim \frac{\nu^{1/2}t^{1/2}}{H} \sim \mathrm{Pr}^{1/2}\;\delta_T \sim \frac{\mathrm{Pr}^{1/2}\;\tau^{1/2}}{\mathrm{Ra}^{1/4}}, \tag{35}$$

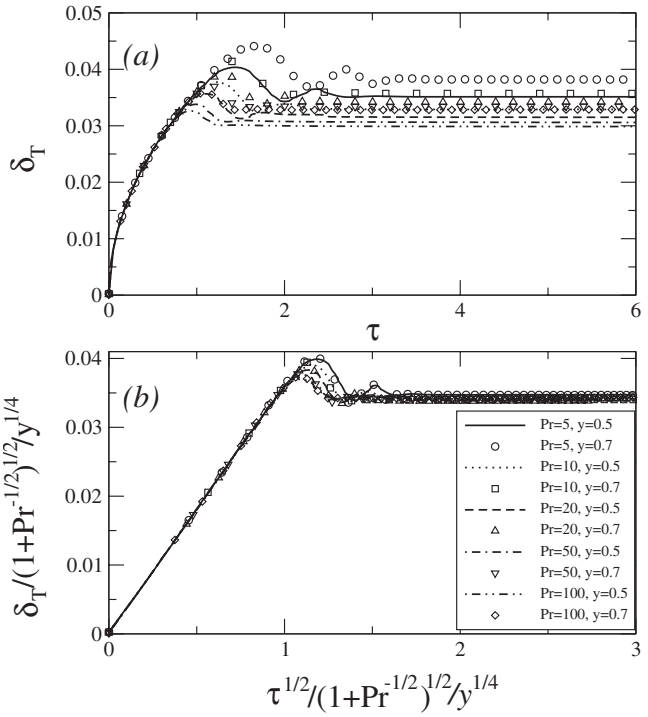

FIG. 5. Time series of dimensionless δ_T at dimensionless heights $y=0.5$ and $y=0.7$ for different Pr: (a) raw data and (b) $\delta_T/[(1+\mathrm{Pr}^{-1/2})^{1/2}y^{1/4}]$ (dimensionless) plotted against $\tau^{1/2}/[(1+\mathrm{Pr}^{-1/2})^{1/2}y^{1/4}]$ (dimensionless).

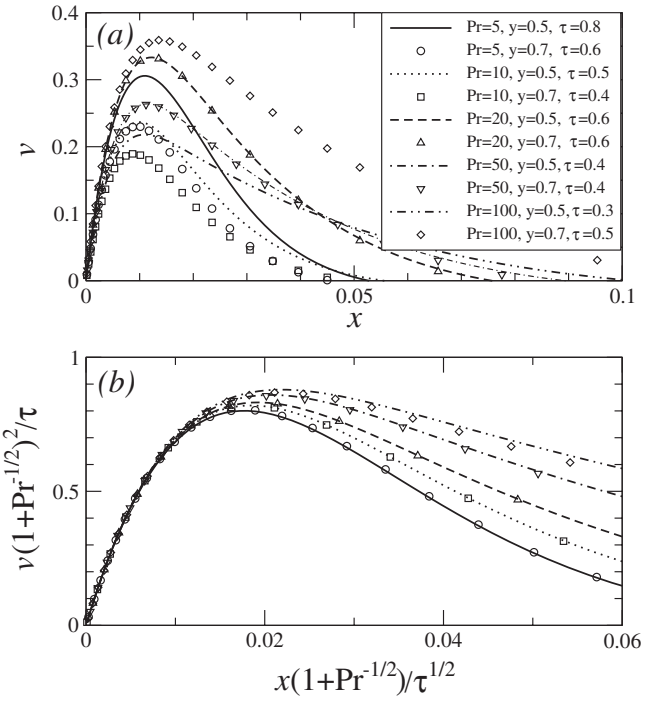

FIG. 6. Horizontal profiles of dimensionless vertical velocity v at dimensionless heights $y=0.5$ and $y=0.7$ for different Pr at the start-up stage: (a) raw data and (b) $v(1+\mathrm{Pr}^{-1/2})^2/\tau$ (dimensionless) plotted against $x(1+\mathrm{Pr}^{-1/2})/\tau^{1/2}$ (dimensionless).

$$\delta_{vi} = \frac{\Delta_{vi}}{H} \sim \frac{1}{1+\mathrm{Pr}^{-1/2}} \frac{\kappa^{1/2} t^{1/2}}{H} \sim \frac{1}{1+\mathrm{Pr}^{-1/2}} \delta_T \sim \frac{1}{(1+\mathrm{Pr}^{-1/2})} \frac{\tau^{1/2}}{\mathrm{Ra}^{1/4}}, \tag{36}$$

$$v_m = \frac{V_m}{V_0} \sim \frac{\mathrm{Ra}\kappa^2}{H^3} \frac{1}{(1+\mathrm{Pr}^{-1/2})^2} \frac{t}{V_0} \sim \frac{\mathrm{Ra}\kappa^2}{H^3} \frac{1}{(1+\mathrm{Pr}^{-1/2})^2} \frac{(H/V_0)\tau}{V_0} \sim \frac{\tau}{(1+\mathrm{Pr}^{-1/2})^2}. \tag{37}$$

The dimensionless form of scaling (24) for t_s is

$$\tau_s = \frac{t_s}{(H/V_0)} \sim \frac{H^2}{(H/V_0)\mathrm{Ra}^{1/2}\kappa} \left(\frac{Y}{H}\right)^{1/2} (1+\mathrm{Pr}^{-1/2}) \sim (1+\mathrm{Pr}^{-1/2}) y^{1/2}. \tag{38}$$

At steady state, scalings (26), (28), (27), and (25) are written in the following dimensionless forms:

$$\delta_{Ts} = \frac{\Delta_{Ts}}{H} \sim \frac{y^{1/4}}{\mathrm{Ra}^{1/4}} (1+\mathrm{Pr}^{-1/2})^{1/2}, \tag{39}$$

$$\delta_{vs} = \frac{\Delta_{vs}}{H} \sim \frac{y^{1/4}}{\mathrm{Ra}^{1/4}} \mathrm{Pr}^{1/2} (1+\mathrm{Pr}^{-1/2})^{1/2}, \tag{40}$$

$$\delta_{vis} = \frac{\Delta_{vis}}{H} \sim \frac{y^{1/4}}{\mathrm{Ra}^{1/4}} \frac{1}{(1+\mathrm{Pr}^{-1/2})^{1/2}}, \tag{41}$$

$$v_{ms} = \frac{V_{ms}}{V_0} \sim \frac{1}{(1+\mathrm{Pr}^{-1/2})} y^{1/2}. \tag{42}$$

Scalings (34)–(37) clearly show that at the start-up stage, the boundary layer development on the vertical plate is one dimensional and independent of y due to the dominance of pure conduction. However, at steady state, as shown by scalings (39)–(42), the boundary layer is two dimensional and y dependent as the flow is now dominated by convection.

IV. NUMERICAL RESULTS AND DISCUSSIONS

In this section, the scalings obtained above will be validated and analyzed by comparison to direct numerical simulation results. These simulations are conducted using the same code as used in [7,11,16,17]. As the numerical methods, the construction of the computational meshes and the benchmarking of the code with known theoretical results were detailed in [16,17], these will not be repeated here.

As the Ra dependence of the scalings for natural convection boundary layers has been firmly confirmed by numerous numerical results (see, e.g., [6–11,16]), this study will focus on the Pr and y dependence of the scalings obtained above. To do so, five direct numerical simulations with varying Pr (specifically Pr=5, 10, 20, 50, and 100, respectively) have been chosen, all at the same Rayleigh number ($\mathrm{Ra}=10^8$).

All the simulations have been conducted in a 2×1 computational domain with 493×397 nodes. To ensure the simulation results are mesh independent, a mesh dependence test has been conducted for the Pr=50 case with three meshes

(493×397, 323×263, and 209×165) for the 2×1 computational domain and one mesh (499×397) for the 4×1 computational domain, and the results are shown in Fig. 2, which clearly demonstrates that the numerical simulation results with finer meshes are mesh independent and domain size independent. Hence, the 493×397 mesh has been chosen for all the simulations conducted in the 2×1 computational domain in this study.

As shown by scaling (34), the dimensionless thermal boundary layer thickness, δ_T, grows as $\delta_T\sim\tau^{1/2}$ at the start-up stage, and shows no dependence on Pr or y. This is clearly confirmed by the numerical results, as depicted in Fig. 3, where the horizontal temperature profiles for different Pr at $y=0.5$ and $y=0.7$ during the start-up stage are presented. Figure 3(b), where x is scaled by $\tau^{1/2}$, which is the scale for δ_T at the start-up stage, shows that this scale brings all ten scaled temperature profiles with the Pr and y variations at different times into a single profile, indicating that $\delta_T\sim\tau^{1/2}$ is the correct scaling for δ_T at the start-up stage.

When the boundary layer development attains its steady state, scaling (39) shows that the boundary layer becomes two dimensional and the dimensionless thermal boundary layer thickness, δ_{Ts}, becomes both Pr and y dependent. This scaling is also confirmed by the numerical results, as shown in Fig. 4, where the horizontal temperature profiles for different Pr at $y=0.5$ and $y=0.7$ at steady state are presented. Figure 4(b), where x is scaled by $y^{1/4}(1+\mathrm{Pr}^{-1/2})^{1/2}$, which is the scale for δ_{Ts} at steady state, shows that this scale brings all ten scaled temperature profiles with the Pr and y variations at steady state essentially onto a single line, confirming that scaling (39) is the correct scaling for δ_{Ts} at steady state.

To more explicitly validate scalings (34), (38), and (39), the time series of δ_T for different Pr at $y=0.5$ and $y=0.7$ have been obtained from the numerical simulations and are presented in Fig. 5. δ_T at a specific height is determined in the simulations as the distance from the vertical sidewall to the location where θ, the dimensionless temperature of the fluid, becomes 0.01. Figure 5(b) presents the same ten time series as those presented in Fig. 5(a), but δ_T and τ are scaled by $(1+\mathrm{Pr}^{-1/2})^{1/2}y^{1/4}$ and $(1+\mathrm{Pr}^{-1/2})^{1/2}y^{1/2}$, which are the scales for δ_{Ts} and τ at steady state, respectively, as shown in Eqs. (38) and (39). At the start-up stage (before each series attains its individual peak), it is seen that all ten scaled time series, with Pr and y variations, fall onto the same straight line, confirming that $\delta_T\sim\tau^{1/2}/\mathrm{Ra}^{1/4}$ is the correct scaling for δ_T at the start-up stage. At steady state, these scaled series fall approximately onto the same horizontal straight line, which clearly confirms that $\delta_{Ts}\sim(1+\mathrm{Pr}^{-1/2})^{1/2}y^{1/4}/\mathrm{Ra}^{1/4}$ is the correct scaling for δ_T at steady state. Additionally, Fig. 5(b) shows that all ten scaled time series attain their respective peaks at approximately the same scaled time, which also validates scaling (38).

Scalings (36) and (37) predict that the inner viscous boundary layer thickness δ_{vi} and the maximum vertical velocity v_m are Pr dependent but y independent at the start-up stage. These scalings have been validated with the numerical results shown in Fig. 6, where the horizontal profiles of vertical velocity at $y=0.5$ and $y=0.7$ for five Pr values during the start-up stage are presented. From Fig. 6(b), where v and x are scaled, respectively, by $\tau/(1+\mathrm{Pr}^{-1/2})^2$ and $\tau^{1/2}/(1+\mathrm{Pr}^{-1/2})$, which are the scales for v_m and δ_{vi} at the start-up stage, as shown in Eqs. (37) and (36), it is seen that these two scales bring all ten scaled profiles within the inner viscous boundary layers onto a single line at the start-up stage in region I.

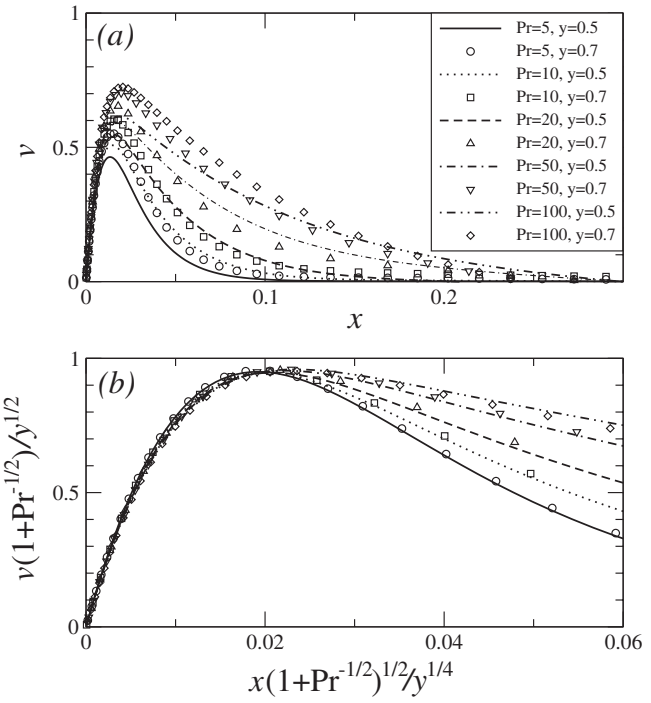

FIG. 7. Horizontal profiles of dimensionless vertical velocity v at dimensionless heights $y=0.5$ and $y=0.7$ for different Pr at steady state: (a) raw data and (b) $v(1+\mathrm{Pr}^{-1/2})/y^{1/2}$ (dimensionless) plotted against $x/[\mathrm{Pr}^{1/2}(1+\mathrm{Pr}^{-1/2})^{1/2}y^{1/4}]$ (dimensionless).

At steady state, the viscous boundary layer also becomes two dimensional and Pr and y dependent, as indicated by scalings (41), (42), and (38). These scalings are also validated by the numerical results, as demonstrated in Fig. 7, where the horizontal profiles of vertical velocity at $y=0.5$ and $y=0.7$ for different Pr at steady state are presented. From Fig. 7(b), where the scaled profiles are presented with v and x scaled, respectively, by $y^{1/2}/(1+\mathrm{Pr}^{-1/2})$ and $y^{1/4}/(1+\mathrm{Pr}^{-1/2})^{1/2}$, which are the scales for v_{ms} and δ_{vis} at steady state, it is clearly seen that these two scales essentially bring all ten scaled profiles within the inner viscous boundary layers onto a single line at steady state, confirming scalings (41) and (42).

Figure 8 presents further numerical results to validate scalings (37), (42), and (38), where the time series of v_m for different Pr at $y=0.5$ and $y=0.7$ are presented. Figure 8(b) presents the same ten time series as those present in Fig. 8(a), but v_m and τ are scaled, respectively, by $y^{1/2}/(1+\mathrm{Pr}^{-1/2})$ and $(1+\mathrm{Pr}^{-1/2})^{1/2}y^{1/2}$, which are the scales for v_{ms} and τ at steady state respectively, as shown by scalings (38) and (42). It is found that all ten scaled time series fall approximately onto the same straight line at the start-up stage, which confirms that $v_m\sim\tau/(1+\mathrm{Pr}^{-1/2})^2$ is the correct scaling for v_m at the start-up stage. At steady state, it is seen that all scaled time series fall essentially onto the same horizontal straight line, which clearly confirms that $v_{ms}\sim y^{1/2}/(1$

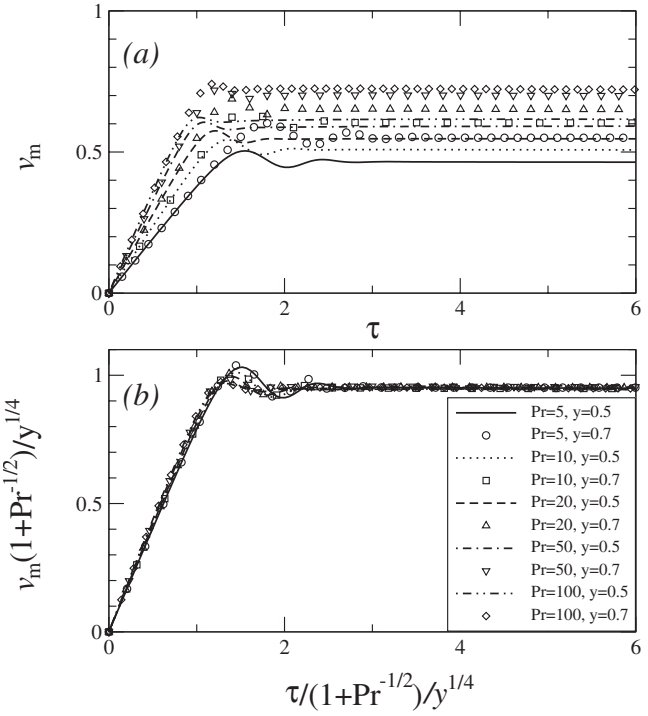

FIG. 8. Time series of dimensionless v_m at dimensionless heights $y=0.5$ and $y=0.7$ for different Pr: (a) raw data and (b) $v_m(1+\mathrm{Pr}^{-1/2})/y^{1/2}$ (dimensionless) plotted against $\tau/[(1+\mathrm{Pr}^{-1/2})y^{1/2}]$ (dimensionless).

$+\mathrm{Pr}^{-1/2})$ is the correct scaling for v_{ms} at steady state. Additionally, Fig. 8(b) shows that all ten scaled time series attain their respective peaks at approximately the same scaled time, which also validates scaling (38).

From the above numerical validation, it is clear that the scalings representing the thermal boundary layer development agree very well with the numerical results with Pr variation over the whole stage of development demonstrating that the Pr dependence of this flow is quite accurately represented. The scalings representing the viscous boundary layer development are generally in good agreement with numerical results with Pr variation over the whole stage of development, although there are small deviations from the numerical results that are within acceptable limits for scaling. As all scalings were obtained under a series of assumptions regarding the relative magnitudes of various terms in the temperature and momentum equations, it will be justifiable to have an examination of these assumptions using numerical results.

To do so, the numerical results obtained for $\mathrm{Ra}=10^8$ and $\mathrm{Pr}=10$ at the specific height of $y=0.5$ are present in Figs. 9 and 10, which present the snapshots of the horizontal profiles of various terms in the dimensionless temperature Eq. (32) and dimensionless y momentum Eq. (31). For this specific case, the numerical results show that the start-up stage completes at around $\tau=1.3$, and after around $\tau=2$, the flow reaches its steady state.

In the scaling analysis, it is assumed that, at the early start-up stage, the temperature Eq. (4), or more appropriately here, its dimensionless counterpart [Eq. (32)], is dominated by the unsteady term and the heat conduction term for $\mathrm{Pr}\gg 1$ fluids and all other terms in the equation are negligible.

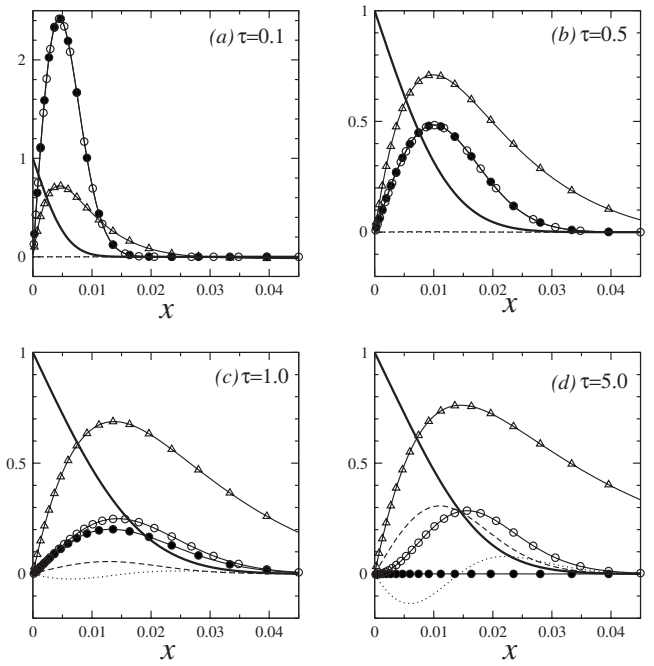

FIG. 9. Snapshots of horizontal profiles of various terms (dimensionless) in the temperature equation at dimensionless height $y=0.5$ for $\mathrm{Pr}=10$ and $\mathrm{Ra}=10^8$. —●— $\partial\theta/\partial\tau$, ····· $\partial(u\theta)/\partial x$, – – – $\partial(v\theta)/\partial y$, –○– $\mathrm{Ra}^{-1/2}\partial^2\theta/\partial x^2$, — (bold) θ, —△— $1.5v$. Note that $\mathrm{Ra}^{-1/2}\partial^2\theta/\partial y^2$ is negligible so it is not present. Also note that the velocity profiles (—△—) at $\tau=0.1$ and $\tau=0.5$ are for $15v$ and $3v$, respectively.

The numerical results in Fig. 9(a) exactly demonstrate this behavior. When τ continues to increase, as shown in Fig. 9(b), these two terms still dominate the temperature Eq. (4), although their magnitudes decrease dramatically, and all other terms are again negligible. In fact, the numerical results, as shown in Fig. 9(c), demonstrate that these two terms continue to dominate the temperature Eq. (32) until the end of the start-up stage, when other terms, such as $\partial(u\theta)/\partial x$ and $\partial(v\theta)/\partial y$, begin to become significant. This well maintained dominance of the unsteady-conduction balance over the whole start-up stage ensures the accuracy of scaling (6) and its dimensionless counterpart [Eq. (34)], as observed above. At steady state, as shown in Fig. 9(d), the unsteady term disappears, which is expected. Nevertheless, the numerical results show that although the two terms that become dominant in the temperature Eq. (32) are $\partial(v\theta)/\partial y$ and $\mathrm{Ra}^{-1/2}\partial^2\theta/\partial y^2$, which is exactly what is assumed in the scaling analysis, the magnitude of the term $\partial(u\theta)/\partial x$ is not negligible. However, its contribution is small, as clearly demonstrated by the numerical results presented in Figs. 3–5.

As observed above, there are small deviations associated with the Pr variation for the scalings representing the viscous boundary layer development, although these deviations are within acceptable limits for scaling. In the scaling analysis, it was assumed that over the whole stage of flow development, the y momentum Eq. (3), or more appropriately here, its dimensionless counterpart [Eq. (31)], is dominated by the viscous term and the buoyancy term for $\mathrm{Pr}\gg 1$ fluids, both in region I (inner viscous boundary layer) and in region II (the

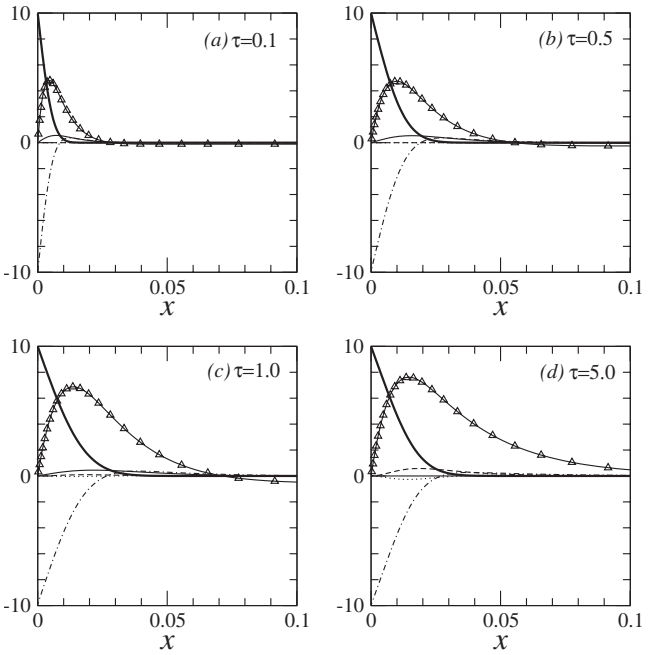

FIG. 10. Snapshots of horizontal profiles of various terms (dimensionless) in the vertical momentum equation at dimensionless height $y=0.5$ for $\mathrm{Pr}=10$ and $\mathrm{Ra}=10^8$. — $\partial v/\partial \tau$, $\cdots\cdots$ $\partial(uv)/\partial x$, – – – $\partial(vv)/\partial y$, – – $\mathrm{Pr}\,\mathrm{Ra}^{-1/2}\partial^2 v/\partial x^2$, — (bold) Pr θ, —△— $15v$. Note that both $\partial p/\partial y$ and $\mathrm{Pr}\,\mathrm{Ra}^{-1/2}\partial^2 v/\partial y^2$ are negligible so they are not present. Also note that the velocity profiles (—△—) at $\tau=0.1$ and $\tau=0.5$ are for $100v$ and $20v$, respectively.

remaining viscous boundary layer within the corresponding thermal boundary layer). This is confirmed by the numerical results presented in Fig. 10, where it is seen that the viscous term $\mathrm{Pr}\,\mathrm{Ra}^{-1/2}\partial^2 v/\partial x^2$ and the buoyancy term Pr θ are the only dominating terms in Eq. (31) at all the times considered, and all other terms are negligible. Hence, this viscosity-buoyancy balance assumption in regions I and II is valid and accurate.

V. CONCLUSIONS

A three-region scaling has been developed to account for the Prandtl number dependency of the developing and fully developed structure of the natural convection boundary layer in a $\mathrm{Pr}>1$ fluid adjacent to an impulsively heated isothermal semi-infinite vertical plate. This scaling shows a strong Prandtl number dependency in the characteristic quantities for the velocity in both the start-up y-independent conductive phase and in the fully developed y-dependent convective phase. However, when Pr approaches infinity, the Pr dependency shown in the scalings will disappear.

The scalings have been validated by comparison to full numerical solutions of the governing equations and have been shown to provide an accurate description of the start-up flow, the transition times, and the structure of the fully developed flow over the Prandtl number range considered. In particular the multiple region scaling accurately predicts the Prandtl number dependency of the inner velocity length scale, δ_{vi}, and the velocity maximum v_m, quantities that are poorly predicted using a single region scaling.

ACKNOWLEDGMENTS

The authors gratefully acknowledge the support of the Australian Research Council. W.L. also gratefully acknowledges the support of the National Natural Science Foundation of China (Grant No. 50879074), the National Basic Research Program of China (Grant No. 2007CB216405), and the Science Research Foundation of Yunnan Provincial Education Department (Grant No. 07Z10378).

[1] I. Catton, *Proceedings of the Sixth International Heat Transfer Conference, Toronto, 1978*, Vol. 6, p. 13.
[2] S. Ostrach, *Proceedings of the Seventh International Heat Transfer Conference, Munchen, 1982*, Vol. 1, p. 365.
[3] B. Gebhart, Y. Jaluria, R. L. Mahajan, and B. Sammakia, *Buoyancy-Induced Flows and Transport* (Hemisphere, New York, 1988).
[4] J. M. Hyun, Adv. Heat Transfer **24**, 277 (1994).
[5] R. J. Goldstein *et al.*, Int. J. Heat Mass Transfer **48**, 819 (2005).
[6] J. C. Patterson and J. Imberger, J. Fluid Mech. **100**, 65 (1980).
[7] W. Lin, S. W. Armfield, and J. C. Patterson, J. Fluid Mech. **574**, 85 (2007).
[8] W. Lin and S. W. Armfield, Int. J. Heat Fluid Flow **22**, 72 (2001).
[9] W. Lin and S. W. Armfield, Phys. Rev. E **72**, 016306 (2005).
[10] S. W. Armfield, J. C. Patterson, and W. Lin, Int. J. Heat Mass Transfer **50**, 1592 (2007).
[11] W. Lin, S. W. Armfield, and J. C. Patterson, Int. J. Heat Mass Transfer **51**, 327 (2008).
[12] J. C. Patterson, C. Lei, S. W. Armfield, and W. Lin, Int. J. Thermal Sci. (to be published).
[13] T. Aberra, S. W. Armfield, and M. Behnia, Proceedings of the CHT-08, ICMHMT International Symposium on Advances in Computational Heat Transfer, (2008), Vol. 13, p. CHT-08–363.
[14] S. W. Armfield and J. C. Patterson, J. Fluid Mech. **239**, 195 (1992).
[15] W. Schopf and J. C. Patterson, Int. J. Heat Mass Transfer **39**, 3497 (1996).
[16] W. Lin and S. W. Armfield, Int. J. Heat Mass Transfer **42**, 4117 (1999).
[17] W. Lin, Ph.D. thesis, The University of Sydney, Sydney, 2000 (unpublished).